Boyatzis *et al. Herit Sci (2016) 4:13*
DOI 10.1186/s40494-016-0083-4

Heritage Science

RESEARCH ARTICLE Open Access

A study of the deterioration of aged parchment marked with laboratory iron gall inks using FTIR-ATR spectroscopy and micro hot table

Stamatis C. Boyatzis*, Georgia Velivasaki and Ekaterini Malea

Abstract

A great number of historic manuscripts, drawings, etc., many of which are stored and/or exhibited in museums, archives and various collections contain iron gall inks (IGIs) as base scripting material. Although the severe deterioration effect of IGIs on paper has been recognized and its chemistry has been explored, little focus has been given on IGIs on parchment. A study was designed to investigate laboratory iron gall inks containing ferrous sulphate and gallic acid (LIG formulation) and with added quantities of gum arabic (LIGG formulation). Specimens marked with the above ink types were artificially aged at 80 °C and 80 % RH for up to 32 days. Micro hot table (MHT) thermal analysis showed a decrease in the shrinkage temperatures in inked areas of aged parchment of up to 15.5 °C. Results of FTIR-ATR spectroscopy showed intense migration of sulphate ions from inked spots to neighbouring ink-free areas at the surface of parchment in both ink formulations, also confirmed by SEM microanalysis results. This effect peaked at short-moderate times of artificial ageing, where calcium sulphate was identified and located at the surface of ink-free areas. Moreover, early signs for gelatinization of collagen also resulted from analysis of Amide I and II infrared bands, where the random coil content increased upon ageing as compared to the helical one.

Keywords: Parchment, Deterioration, Iron gall ink, Shrinkage temperature, Infrared spectroscopy, Amide I, Amide II, Secondary structure, Peak fitting

Background

Parchment is an important archival material, mostly used as support for writing and illuminations, as well as structural material (book binding, etc.). Historically, parchment was officially introduced in the city of Pergamum around the 2nd century A.D., although there is evidence for earlier uses [1, 2]. Since then, it has been the main material for writing until the emergence of handmade paper. Parchment artefacts, such as the Dead Sea Scrolls, The Vinland Map and J. S. Bach manuscripts have been the research focus for conservators and conservation scientists, investigating deterioration pathways and effective methods for conservation [3–7]. These studies provided insight regarding the parchment deterioration routes and mechanisms [8–10].

Iron gall inks (IGI's), were first used during the middle ages on both parchment and paper. Numerous artists and scholars expressed their mastery in iron gall ink, using either medium. However, IGI's are notoriously known for inducing severe deterioration mainly on paper, and therefore, a large number of studies have been focused on understanding and potential reversing this effect. IGI's on parchment have received considerably less attention as the interaction between the two materials is not directly explored, although a significant amount of research has been undertaken separately on these media [6]. A great amount of inked, or illuminated parchment artifacts are stored and/or exhibited in museums, libraries, private collections, archives, etc., and a great deal of these are in serious state of degradation. However, it is basically

*Correspondence: sboyatzis@teiath.gr
Department of Conservation of Antiquities & Works of Art, Technological Educational Institution of Athens, 12210 Egaleo, Greece

unclear to what extent these have been affected by the presence of IGIs.

Regarding IGI terminology, recipes that rely on a great variety of natural ingredients, are acceptably termed as historic iron gall (or HIG) inks. On the other hand, inks based on simple formulations, or the chemically active materials that are actually needed, are called laboratory iron gall (or LIG) inks.

Parchment

Parchment is a post mortem tissue, composed mainly of collagen type I. It has been traditionally produced from animal skins, such as goat, sheep, cow, camel, etc., after a manufacturing process that varies according to geographical locations, which mainly includes processing with soaking, liming, unhairing, fleshing and drying [11]. As a result, residual quantities of chemicals, more importantly calcium carbonate (as the result of lime exposure to atmospheric carbon dioxide) are evident. Other inorganic and organic substances may be found such as alum, silicates, oils, tannins, etc., which affect the texture and hardness of the material [12, 13]. Significantly, the material that is produced has already a degree of deterioration related to the initial material in animal skin; this includes partial hydrolysis of peptide chains and gelatinization [14–16].

A significant amount of research has been undertaken on collagen and related materials such as gelatin. Some key points of collagen structure include the formation of chains in a left-handed 3.3 helix conformation by a basic amino acid sequence of approximately 1050 amino acids, following the general pattern of Gly-X–Y (where X and Y are mainly proline and hydroxyproline units, also varied by glutamic acid, alanine, arginine, etc.). The helical chains are turned in a way that a right-handed triple helix is formed in a three-dimensional coiled coil geometry [17–19]. Formation of coiled coil is favoured by a staggered packing of trimers, according to which a complex hierarchical structure is maintained; this is responsible for the exceptional stability of the material that nature successfully utilizes as skin, cartilage and bone tissue. Several types of collagen are known, which have various amino acid sequences, and therefore, different structural hierarchies. For instance, type I collagen is a heterotrimer, i.e. its triple helix has two α1 and one α2 helices, while type III is a homotrimer, i.e. it is composed entirely of α1 chains. Formation of fibrils through self-organizing of collagen chains is a significant feature, which only collagens type I, II, III, V and XI possess [15, 20, 21].

A key feature in the stability of collagen fibrils and the overall structural hierarchy is the extended network of hydrogen bonding exerted both among amino acids in adjacent chains within a trimer, and also, between water molecules and certain amino acids in each trimer. At this point, the role of water should be emphasized, as it plays an extremely significant role in the stability of the entire molecule [21–24]. A significant number of water molecules, termed *structural* water, reside inside the triple helix and mediate hydrogen bonds between carbonyl and amino groups from one chain and hydroxyl groups of hydroxyproline units from another, while other water molecules mediate hydrogen bonding between trimers. Finally, helical chains may also cross-link with each other through covalent bonding.

Parchment is composed of type I and type III fibrillar collagen depending on the animal type, body part and age; therefore, the above mentioned complex structure of collagen is also present in parchment [11, 15, 16].

The manufacturing process, as already mentioned, has a detrimental effect at some level on the structure of parchment. Therefore, the material already exists in a partly degraded state in relation to collagen: the various preparation steps (see above) render a material that has significant differences from that in the original skin. This means that any further deterioration of parchment due to light, heat, moisture, etc., in essence takes the cue from already existing defective centers in the material. Notably, acidic hydrolysis may downsize the collagen fibrils seriously altering their conformation and therefore their secondary and tertiary structures. Oxidative degradation affects mainly the functional side groups, i.e. reduces the amine-containing basic amino acids, and increases the acidic ones, while in more extreme conditions cleavage of the C–N bonds in the backbone may occur [15, 25].

On a higher level, factors that have an effect on the structural water molecules may disrupt the tight hydrogen bonding network. This may also happen, aided by any of the hydrolytic or oxidative mechanisms. Uncoiling of the chains in the triple helix to random conformations finally occurs. As chains are now exposed to a denser water environment, hydrogen bonding becomes more intense, significantly affecting spectral characteristics (as a key feature throughout the results in this work, see "Results and discussion" section). As a result of the various degrading processes, the hydrothermal constant of parchment has been shown to change on the structural and molecular levels. Shrinkage temperatures have been observed to decrease upon exposure of parchment to hydrolytic and oxidative environments [9, 26].

Iron gall inks

The chemistry of iron gall inks (IGI's) is complex and only recent studies have contributed to an improved understanding of some aspects including: (a) development of acidic pH, (b) gallic acid hydrolytic formation from tannins, (c) formation of iron (II)—gallate complex, rapidly

oxidizing to insoluble blue-black iron (III)—gallate complex, (d) significant quantity of iron (II) ions remaining in the ink mixture [27–29].

The colour of an iron gall ink depends on the interaction of iron (III) with free gallic acid produced through tannin hydrolysis. As a result, in hydrolysable tannins, iron (III)—gallate coordination complex is responsible for the typical blue-black colour, while the analogous ellagate complex is similarly coloured. On the other hand, complexes of iron with oxidation products of the initial favan-3-ol (or catechin), which are components of non-hydrolysable tannins are brown-green or brown-grey [30, 31]. Moreover, ternary complexes of iron (III) with gallate having various colours have been investigated, also involving amino acids such as glycine. For instance, [iron (III)-gallate] complex absorbs at 560 nm, while the ternary complex [iron (III)-gallate-glycinate] absorbs at 500 nm [28].

At this point, two main structures for the iron (III)—gallate complex have been proposed, one that iron complexes gallic acid through hydroxyls in a 1:1 ratio [32] and another that complexation occurs through both hydroxyl units and carboxylates [33, 34]. Chemical structures are shown in Fig. 1.

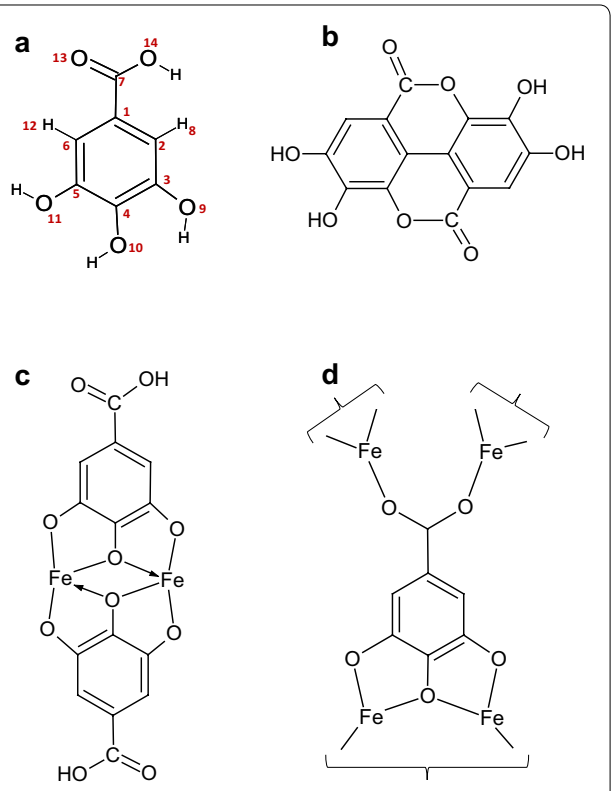

Fig. 1 Chemical structures of **a** gallic acid, **b** ellagic acid, **c** iron (III)—gallate complex proposed by Krekel [32] and **d** iron (III)—gallate complex proposed by Wunderlich [33] (see main text)

Analytical techniques

Fourier transform infrared (FTIR) spectroscopy provides valuable information on the various bonding types within molecules in materials [35]. It has been extensively employed, among others, in studies focusing on changes in materials of cultural heritage due to ageing on the basis that bonding loss or generation are reflected in corresponding changes of specific absorptions in the FTIR spectrum [36, 37]. Attenuated total reflection (ATR) is a sampling technique that with the help of a crystal of high refractive index (usually germanium, diamond or zinc selenide) which is in close contact with the sample surface takes advantage of the total internal reflection phenomenon. In FTIR-ATR spectroscopy, an evanescent infrared wave travels into the crystal with a suitable angle of incidence and penetrates into the sample approximately by 1–3 mm, where part of the radiation is absorbed depending on the bonding in the molecules of the material [38–40].

Infrared spectra of proteinaceous materials are characterized by a general pattern in which, main features are the Amide A band (absorbing at 3400–3100 cm^{-1}; assigned to first component of Fermi resonance between N–H stretch and the overtone of Amide II), Amide B (3080–3050 cm^{-1}; assigned to the second component of Fermi resonance between N–H stretch and the overtone of Amide II), Amide I (at 1670–1620 cm^{-1}; assigned to carbonyl stretch with contributions from C–N stretch and N–H bend), Amide II (at 1570–1520 cm^{-1}; assigned to coupling between N–H bend and C–N stretch) and Amide III (1240–1200 cm^{-1}; assigned to coupling between C–N stretch and N–H bend with contributions from C=O in-plane bend and C–C stretch) [24, 41]. Band assignments for collagen and related materials fall within this pattern [42, 43]; maxima are shown in Fig. 5, while assignments can be found in Table 1. To the above bands, infrared absorptions of hydrocarbon groups, as well as those of functional side groups of amino acids such as glutamic and aspartic acid, may be added; absorptions of acidic side chains depend heavily on the current pH of the material [44].

Moreover, additional information about the conformation of the protein secondary structure can be obtained through deconvolution of the relatively broad Amide I, II and III bands. The Amide I is the most extensively studied mode [45, 46] exhibiting a typical band profile, with the envelope shape depending on the actual molecular environment of the absorbing amide carbonyl bond. Further analysis of the Amide I band can be performed through spectral subtraction, second derivative, Fourier deconvolution and peak fitting [39, 47]. As is the case with most proteins, deconvolution and peak fitting can be applied on the basis of band broadening due to various

Table 1 Assignment of main infrared peaks (cm^{-1}) of standard materials and compounds

Absorption maximum (cm^{-1})		Assignment*
Collagenous materials		
Collagen	Parchment	
3315 s, br	3302	Amide A: first component of vN–H in Fermi resonance with the amide II overtone (overlapping with v_{as}O–H (3447 br) and v_sO–H (3240 br) of structural H_2O)
3072, m–w, br	3072	Amide B: (second component of vN–H in Fermi resonance with the amide II overtone)
2958	2926	*v*C–H
1640 s	1644	Amide I: *v*C=O with small contributions from vC–N and *δ*N–H)* [overlapping with δH–O–H (approx. 1610) of structural H2O]***
1545 s	1538	Amide II: (*v*C–N with contributions from δ_{ip}N–H)**
1454 m–w	1448	δCH_2 of Pro-
1405 w	1408	δ_{ip}C–O–H (carboxylic side chains) and δNH_2
1340 w	1334	wCH_2/δC–H (methine)
1241 m–w	1230	Amide III: (vC–N + *δ*N–H with contributions from vC–C and δ_{ip}C=O)**
1082, 1032	1084, 1031	Breathing of proline ring [69] with carbohydrate vC–O and vC–O–C (glycosylation sites) [70]/parchment: additional esters [66]
Gallic acid [40, 73, 74]		
3498		vO_9H, $vO_{11}H$
3366		$vO_{10}H$
3284		$vO_{14}H$ (COOH)
3065, 2996, 2844		vC_2–H, vC_6–H
2673, 2632, 2575, 2512		$vO_{14}H$ (–COOH dimers)
1703		*v*C=O
1668, 1648		*v*C=O (–COOH dimers)
1612,1542,1484, 1468, 1427, 1387, 1321		*v*C=C (aromatic ring vibrations)
1268		*v*C–O
1221		*δ*(i–p) C–O–H
1184		vC_1–C_7 + *v*C–H
1099		vC_1–C_7 + *δ*C–O–H
1028		Aromatic *asym-*, *sym-* breathing, vC_1–C_7 + *v*C–OH (phenol)
904		*v*C–O + *δ*(o–o–p) C–O–H (dimer band) + *δ*(o–o–p) of ring
867		*δ*(i–p) C–H
767		*δ*(o–o–p) C–H (out-of-phase)
735		*δ*(o–o–p) C–H (out-of-phase) + *τ*C–OH (torsion)
703		Aromatic ring puckering
636		Aromatic ring puckering + *δ*(o–o–p) C–O–H (phenolic)
559		*δ*(o–o–p) C–O–H (phenolic)
492		*τ*C—aromatic ring
Gum Arabic		
3352		*v*OH
2932		*v*C–H
1604		$v_{as}COO^-$
1418		v_sCOO^-
1146(sh), 1068, 1035(sh)		*v*C–O
Iron (II) sulfate heptahydrate		
3336		*v*OH
1652		*δ*OH in water
1092		v_1 SO_4^{2-}
977		v_3 SO_4^{2-}
619		v_4*(asym-)* SO_4^{2-}
LIG ink formulation		
3415		*v*OH in water
1645		*δ*OH in water
1094		v_1 SO_4^{2-}
977		v_3 SO_4^{2-}
628		v_4*(asym-)* SO_4^{2-}
LIGG ink formulation		
3439		vH–O in polysaccharide (gum Arabic) and water
2931		*v*C–H
1640		*δ*OH in water overlapping with $v_{as}COO^-$ in polysaccharide (gum Arabic)
1424		v_sCOO^- in gum Arabic
1083		v_1 SO_4^{2-} overlapping with *v*C–O in gum Arabic
1146(sh), 1035(sh)		*v*C-O in gum Arabic
604		v_4*(asym-)* SO_4^{2-}

* *v* stretching; *δ* bending; *d* deformation; *ip* in-plane; *sh* shoulder

** According to Refs [24, 41]

*** According to Ref [24]

components with similar vibrational energies due to variable extent of hydrogen bonding between corresponding NH and C=O groups of adjacent chains within the triple helix, beta sheets and random coils. This technique has been extensively used and is based on the statistical convergence of convoluting curves within a band envelope [48].

Thermal analysis has been employed in the characterization of materials like leather and parchment [49–52]. Damaged parchment has been successfully assessed through visual microscopic observation of heated humid samples and investigating the shrinkage temperatures (T_s) using a micro hot table (MHT) [26, 53–55]. This is based on the ability of collagen-based fibers, such as leather and parchment to deform upon heating in water. More specifically, the two materials in wet state are known to shrink in a temperature regime which depends on their degradation level.

The success of the technique lies in its simplicity, and on the fact that the observed transitions are in good

accordance with other thermal techniques, such as differential scanning calorimetry (DSC). For instance, the T_s values of parchment in a fresh state are in the range of 55–60 °C, while those of heavily damaged parchment are lower, at 30–40 °C.

In the case of inked parchment, SEM-EDX microanalysis can also be helpful because inorganic components may be traced through the elemental composition of surfaces and cross sections of the material.

Aims of this work

This work focuses on the effect of laboratory iron gall inks in parallel with artificial ageing involving moderate heating (80 °C) and humidity (80 % RH) on the parchment state. Chemical characterisation with FTIR spectroscopy, in conjunction with MHT for thermal analysis and SEM-EDX for elemental microanalysis are employed to investigate changes in the material. A key parameter in this investigation is the combination of these changes with molecular information gained mainly from FTIR-ATR spectroscopy. A number of simultaneous chemical processes involving iron gall inks on parchment may occur: potential acidic hydrolytic degradation of parchment [15] and iron (III)—mediated oxidation of the organic substrate in a fashion analogous to paper [56, 57]; on the other hand, tannins contained in ink formulations may interact with collagen towards a stabilized medium [58–60]. Therefore, any investigation undertaken on parchment marked with iron gall inks is nevertheless expected to involve counter-acting phenomena which complicate analytical observations. For this reason, a simple laboratory ink formulation involving no actual tannin, but simply based on gallic acid, was employed and applied by marking on parchment substrate. The basic formulation contains iron (II) sulphate and gallic acid as main ingredients with two variations: one with added gum arabic and the other without.

The shrinkage temperature (T_s) provides very important information for the conservator, as reduced T_s values are significant to material damage and can allow the conservator to make a well-informed decision to the level of intervention that needs to be undertaken. Correlating the T_s values with the types of changes on the structural and molecular level will eventually lead to better assessing the type of damage (i.e. oxidative, hydrolytic cleavage of peptide bonds, gelatinization). A key question arises, as to how successfully the molecular information gained through infrared spectroscopy can be correlated to investigations at the macro- and micro- level and how these may be envisaged as a part of a broader study that includes a great range of related material in cultural heritage [61]. Any changes in intermolecular bonding recorded through FTIR-ATR spectra, occurring in parallel to recorded changes in T_s values, and also differentiate ink-free parchment from inked areas, can be considered a legitimate basis for such correlation.

Results and discussion

Experimental design

Hydrolysis of collagen in the acidic environment that IGIs produce, may degrade collagen fibrils, seriously altering their conformation and therefore their secondary and tertiary structures. These changes are proposed to be evident when analysing the thermal parameters and visual assessment. On the other hand, hydrolysable tannins (for instance, penta- and deca-galloyl glucose) are known to bind to collagen; therefore, in the acidic environment that IGIs achieve, tannin molecules are expected to stabilize parchment in a similar (but to a lesser extent) manner to leather [16, 59].

In light of the above, isolating the two anticipated counter-acting effects and excluding the stabilizing effect due to tannin-collagen binding is essential in order to design an experiment that provides interpretable results. Therefore, a basic laboratory ink formulation was prepared that uses gallic acid as a potential ligand to iron. Binding of gallic acid to parchment collagen is much weaker by comparison to that of a tannin [60, 62–64].

In the absence of a stabilizing effect, changes in the collagenous material are expected to occur and can be measured in terms of the hydrothermal constant (shrinkage temperatures measured by micro-hot table, MHT) and by changes in the protein Amide I and II peaks measured using FTIR-ATR spectroscopy [50, 51, 65].

Laboratory inks were prepared by mixing iron (II) sulphate with gallic acid, while gum arabic was considered as an extra factor (see "Experimental" section). This way, the expected stabilizing effect of tannins was reduced at the most possible level in favour of a more controlled study which better focuses in potentially degrading effects.

The laboratory ink formulation prepared with mixing gallic acid and iron (II) sulphate (LIG ink) produced a weak blue-black solution. The second type of ink in which, gum arabic was added (LIGG ink) resulted in a deep blue-black suspension. Parchment rectangular specimens (each 40 × 0.8 mm approximately), were cut from a single parchment piece and were stained with the prepared inks. In each specimen, three, approximately rectangle, ink-stained zones, separated by non-stained areas were formed (see Fig. 2). Some of these areas were subject to sampling for various analyses (see "Experimental" section).

Visual macroscopic examination showed that all LIGG ink markings on specimens were, as expected, darker-coloured than the LIG ink ones. Interestingly, all

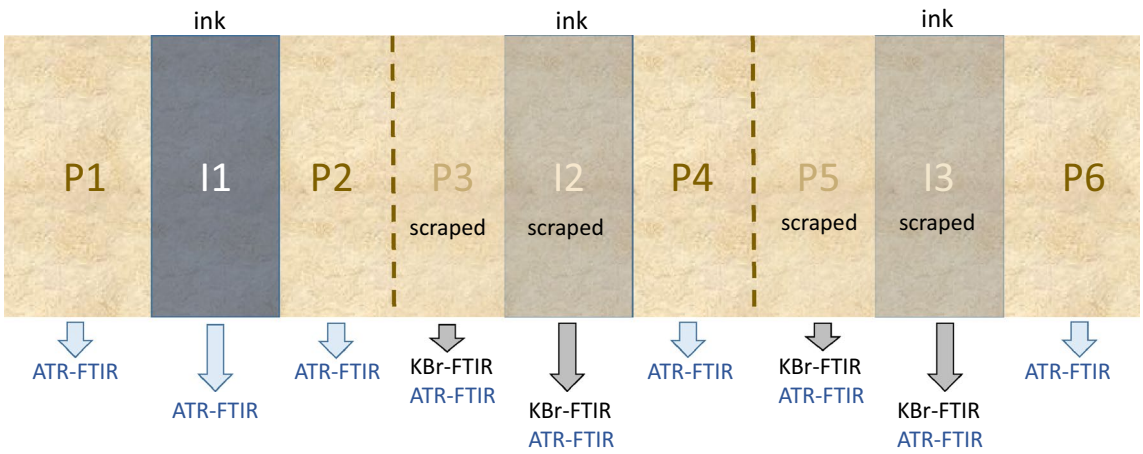

Fig. 2 Schematic of typical parchment specimen designed for this study of inked and ink-free areas. Areas are designated as: I1, PI, P2, P4, P6: ATR-FTIR Analysis. I2, I3, P3, P5: Area sampled to make KBr pellets followed by ATR-FTIR analysis

specimens experienced ink discolouration after ageing as the blue-black tint of inks in all cases changed to brown (see Fig. 3).

Micro hot table (MHT) assessment of parchment degradation

The shrinkage temperatures of micro-samples (in the form of fibres) which were removed from inked and ink-free areas of parchment were investigated using the micro-hot table (MHT) technique (see "Experimental" section) from which, shrinkage temperatures (T_s) were observed.

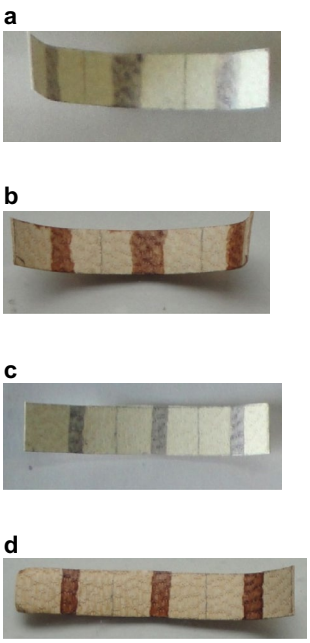

Fig. 3 Photos of parchments specimens inked with laboratory formulations of iron galls inks without gum Arabic (LIG) **a** before and **b** after artificial ageing and with gum Arabic (LIGG) **c** before and **d** after artificial ageing

The shrinkage temperature values of ink-free parchment areas are shown in Fig. 4a and b, where a decrease in T_s is observed. This is expected due to the applied ageing conditions. However, in LIG formulations this decrease occurs as early as the second day of ageing, which is found to happen in parallel to sulphate ion migration from inked areas towards ink-free areas of the parchment surface; this is supported by SEM-EDX and FTIR-ATR data, as discussed in the following sections and seen in Figs. 5, 7, 8, 9 and 10, correspondingly.

Different patterns in the decrease of T_s are also observed in inked areas between LIGG and LIG formulations (Fig. 4). In the former, where gum arabic provides an impeding medium for iron (III), only longer ageing times manage to deteriorate the parchment, with temperature decrease (ΔT) reaching up to 15.5 °C. In LIG formulations, where a more fluid ink medium was applied, deterioration starts earlier, at the second day of ageing, with a ΔT of 8.1 °C, with ΔT reaching up to 12.6 °C at longer times. The graphs in Fig. 4c and d reflect the condition of inked parchment taken from specimens of both ink formulations.

SEM-EDX results

Scanning electron microscopy (SEM) showed extensive crystal formations on the surface of all parchment specimens after ageing (Fig. 5). Energy dispersive X-ray spectrometric (EDX) microanalysis of crystals showed sulphur and calcium within the inked areas, as well as the neighbouring parchment areas; iron was detected in all inked areas, but not in parchment areas, with the exception of small quantities in LIG specimens after 32 days of

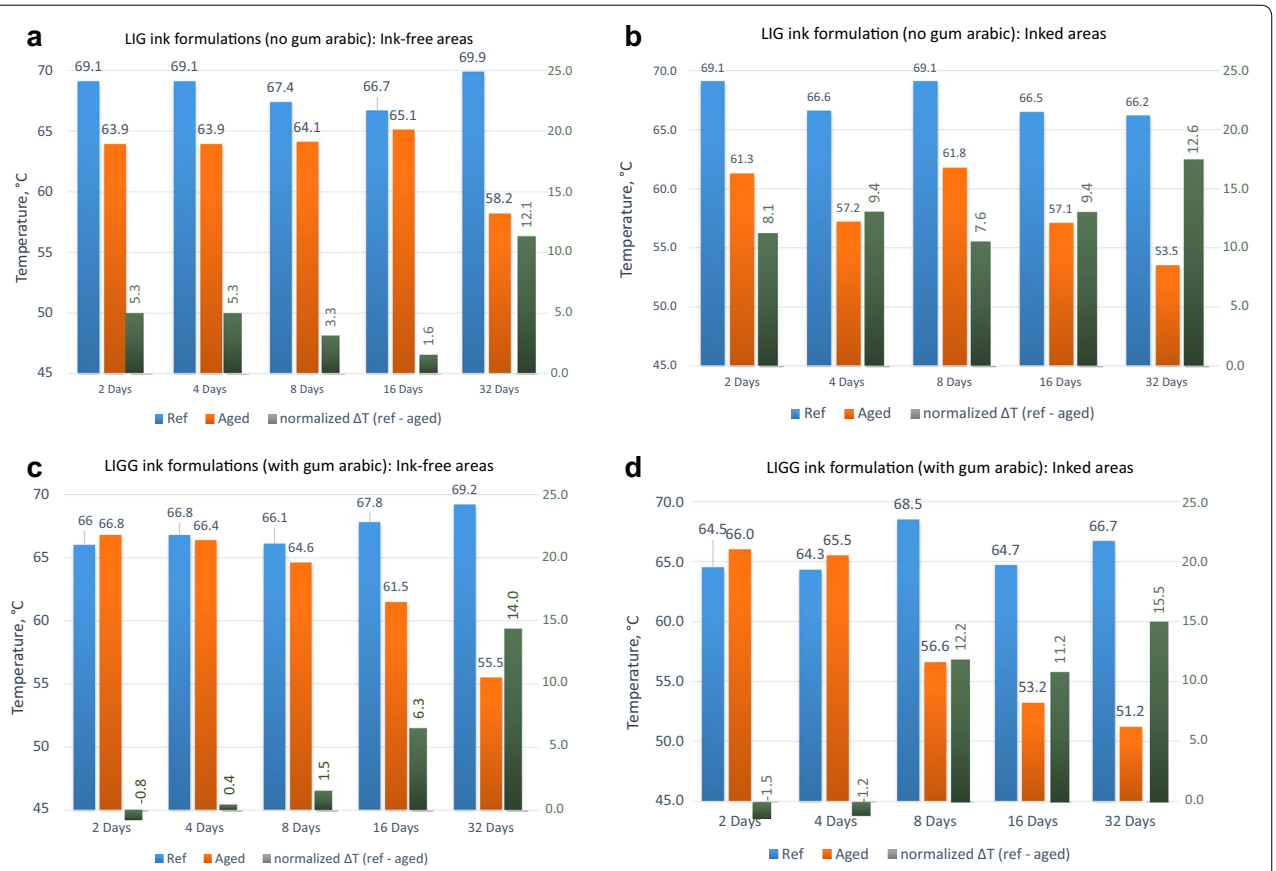

Fig. 4 *Graphs* showing shrinkage temperatures in reference (*blue bars*) and aged specimens (*orange bars*), as well as their corresponding normalised differences (Δ*T*, *green bars*) in **a** ink-free parchment areas (LIG ink formulations); **b** inked parchment areas (LIG ink formulations); **c** ink-free parchment areas (LIGG ink formulations); **d** inked parchment areas (LIGG ink formulations). Temperature differences were normalised with respect to temperatures of reference samples. *Left-hand scale* corresponds to temperatures recorded in reference and aged specimens; *right-hand scale* corresponds to normalised temperature differences (Δ*T*)

artificial ageing. This suggests the migration of sulphate and calcium ions from the initially marked spots towards ink-free areas of the parchment surface. On the contrary, iron ions did not exhibit the same behaviour, as they are bound to the gallate complexes; gallic acid in turn, is expected to bind with gelatinized collagen [60] and this may additionally impede iron mobility. The sulphate and calcium ions eventually precipitate as crystalline calcium sulphate. The presence of sulphate ions in ink-free parchment areas was confirmed by FTIR-ATR spectroscopy (see Fig. 6, the increasing intensity of the absorbances in the 1200–1100 cm^{-1} region, the difference spectrum and corresponding assignments in Table 1). Furthermore, the crystals appeared to be bigger and fewer in number inside ink regions, while those in ink-free parchment areas appeared smaller and denser (Fig. 5).

Infrared spectroscopy results

Mid-infrared spectra of powdered KBr samples collected by scraping selected spots from each specimen (see Fig. 2) were recorded. However, as these samples reflect the bulk properties of parchment in inked and ink-free areas, they do not provide spatial information on the material surface.

FTIR-ATR spectroscopy provided critical information to allow for assessment of the iron gall ink formulations on selected parchment ink spots and neighbouring ink-free regions. Furthermore, selected areas within each specimen that were previously scraped, revealed ageing and inking effects on the underlying layers of the material. This way, information from both the parchment surface and near-surface could be gained.

In order to minimize the effect of spatial variation of a inhomogeneous material, two (and when possible, three) inked spots were analysed together with corresponding ink-free material with a 5 mm distance from the ink mark boundary; all spectra were recorded in this manner to ensure reproducible results and were obtained allowing for a robust comparison of spectra collected from similar areas of different specimens. The viability

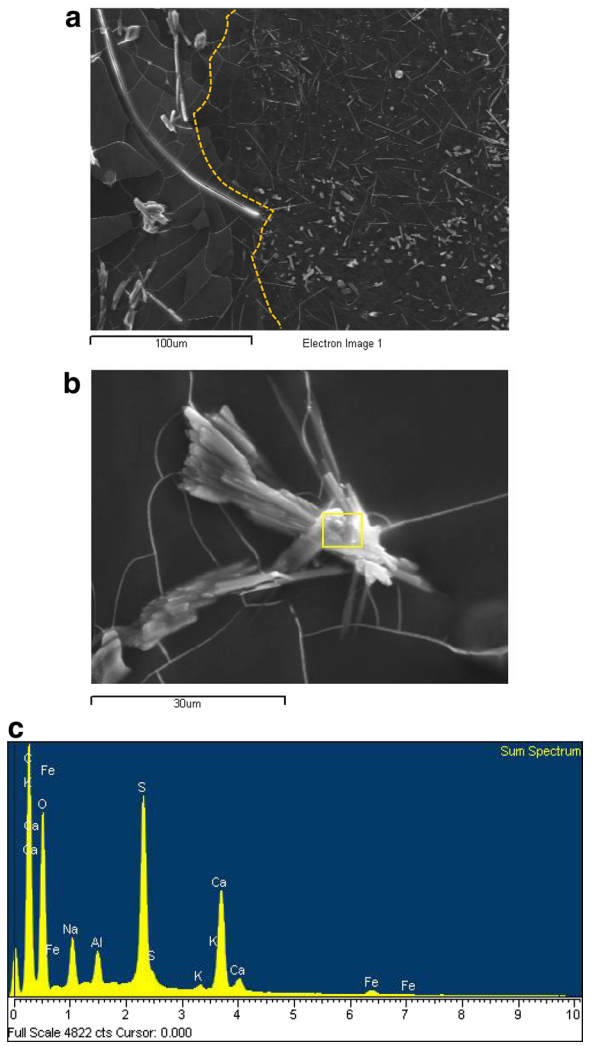

Fig. 5 **a** Electron micrograph with EDX microanalysis of a parchment sample marked with LIGG ink after artificial ageing at 32 days (T = 80 °C, RH = 80 %). *Dotted line* indicates ink region (*left*) and parchment region (*right*). At both regions, $CaSO_4$ crystals are recognizable in varying sizes and quantities; original magnification ×500. **b** Magnified electron micrograph with EDX microanalysis of salt crystal in a LIGG ink region of parchment sample marked with ink after accelerated ageing at 32 days (T = 80 °C, RH = 80 %); original magnification ×2000. **c** Elemental EDX microanalysis spectrum of area in *yellow frame* in 4 (b)

of spectrum-based comparisons between similarly positioned spots of different specimens was thus ensured.

Spectra of initial materials

Figure 6 presents the FTIR-ATR spectra of reference parchment, collagen, gum arabic, iron (II) sulphate, along with spectra of dried samples taken from the LIG and LIGG ink formulations. Peak assignments presented in Table 1. An understanding of the spectral contributions from these individual components helps in the spectral interpretation of the inked and non-inked parchment. Spectra of collagen and parchment are similar, with few exceptions such as the absorption at 1031 cm^{-1} in parchment which is absent in collagen; this can be assigned to aromatic C–C vibrational modes in tannins, and has been proposed as a marker for tannin-processing of parchment [66].

Specimens with LIG formulation

Ink-free areas

The FTIR-ATR spectra recorded from the ink-free areas of all specimens marked with LIG formulation ink are shown in Fig. 7. The most significant change is an increase in a broad peak centred at approximately 1135 cm^{-1}, assigned to the v_3 vibrational mode of calcium sulphate and attributed to migration of sulphates from inked to neighbouring ink-free areas, a phenomenon also observed through scanning electron microscopy and elemental microanalysis (Fig. 5).

Moderate artificial ageing times (2–8 days) are enough for the full extent of migration, where the sulphates absorption peak reaches a maximum. The intensities of these peaks demonstrate the effectiveness of this phenomenon and confirms previous report for such ion migration [16].

The difference spectrum between the longest ageing time (32 days) and the unaged specimens is shown in curve D of Fig. 7a. The peaks at 3525, 3397, 1127, 658 and 600 cm^{-1} reflect changes in the aged specimen and are assigned to sulphates detected as their calcium salt (see Figures S14 and S15 in Additional file 1), which migrated from the neighbouring ink area. In addition, the bands at 1616 and 1508 cm^{-1} reflect changes in Amide I and II bands.

Close examination of the Amide I band (Fig. 7b), shows a decrease in the intensity of the helical components at ~1655 cm^{-1} with increasing ageing times and a relative increase in the contribution of random coils (around 1630 cm^{-1}). This is supported by deconvolution and peak fitting of the spectral region including Amide I and II peaks (Fig. 7c, d), which uncovers two main components centred at ~1658 and ~1629 cm^{-1} corresponding to the helical and random (or uncoiled) components, respectively. A moderate increase of the uncoiled component is observed upon ageing, a possible early sign of change in the medium. Additionally, a component assigned to water (marked by *w*) is also observed in all cases [15, 24].

Collection of the spectra from underlying parchment in ink-free areas was also possible after gently scraping the surface material. No evidence for sulphates migration was observed (spectra not shown), suggesting that migration occurs mainly on the sample surface.

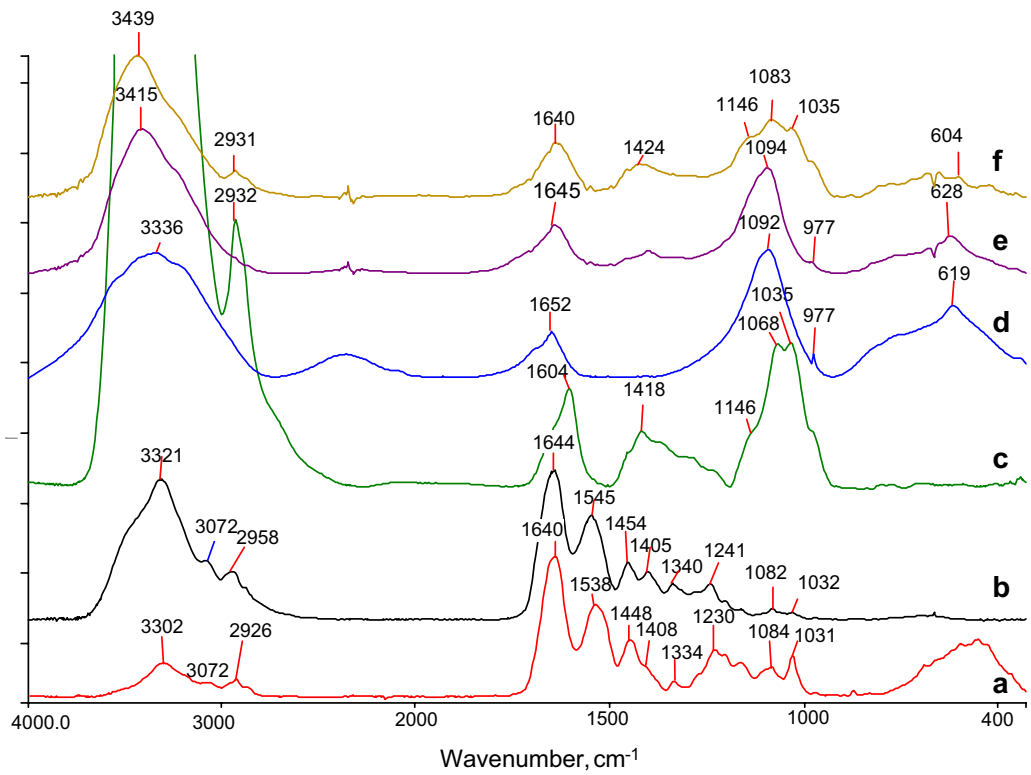

Fig. 6 FTIR spectra of standard compounds and formulations; *a* parchment; *b* collagen; *c* gallic acid; *d* gum arabic; *e* iron (II) sulfate heptahydrate; *f* laboratory iron gall ink from mixing iron (II) sulfate heptahydrate with gallic acid (formulation LIG); *g* laboratory iron gall ink from mixing iron (II) sulfate heptahydrate with gallic acid and gum arabic (LIGG). All spectra shown in absorbance mode. Spectrum a recorded in ATR-FTIR mode; spectrum b recorded on films of the corresponding material on silicon wafer in transmission mode; spectra *c–g* recorded from KBr samples in transmission mode. Spectrum d is shown off scale in the 3600–3000 cm^{-1} area

Inked areas

The FTIR-ATR spectra from inked areas (parchment areas P1 or P2 in Fig. 1) are shown in Fig. 8. The spectra are dominated by the parchment peaks, while those of ink material are largely overlapped. The difference spectrum between inked and ink-free areas of unaged specimens (curve D1 in Fig. 8a) reveals the presence of ink along with its possible interactions with peaks at 1606 cm^{-1} (assigned to the aromatic absorbance of gallate and contributions from water [24]) and 1436 cm^{-1} (assigned to the symmetric stretch of iron (III)—gallate coordination complex [29, 32, 34]). In addition, the peaks at 1217, 1152 and 1087 cm^{-1} can be assigned to vibrations of C–O bonds, including newly formed ester links. The peak at ~1028 cm^{-1}, which is also observed in parchment in its initial state (Fig. 6a) and a marker for tannin pre-processing of the material [66], is significantly increased, suggesting a hitherto unspecified interaction of gallic acid.

Ageing of inked areas did not significantly affect the ferrous sulphate absorption (1300–1000 cm^{-1} region), with the exception of the 4 days' ageing specimen which shows a moderate increase, due to formation of calcium sulphate (maxima at 1154 and 1110 cm^{-1}) at this early stage. On the other hand, a shoulder at 1713 cm^{-1} (possibly due to newly formed acidic carbonyls caused by hydrolysis), and a marked decrease in the intensity of the Amide III region (1235–1200 cm^{-1}) region, are clearly seen in the spectrum of the 32 days' specimen.

The difference spectrum between the inked and ink-free areas of unaged specimen (curve D1 in Fig. 8a) basically corresponds to ink and its possible interactions (aromatics in 1606 and 1508 cm^{-1}, as well as C–O stretching at 1217, 1152, 1087 and 1028 cm^{-1}, discussed above). The difference spectrum between the 32 day-aged and the unaged specimen (curve D2) reveals peaks at ~1608 and ~1429 assignable to the gallate complex, as well as at 1713 cm^{-1} attributed to carboxylic acids.

Deconvolution and peak fitting in the 1780–1480 cm^{-1} region shows the contribution of various components in Amide I band. In the spectrum of the unaged specimen (Fig. 8c), two components are resolved, a helical (1659 cm^{-1}) and an unordered one (1629 cm^{-1}). In addition, the water component in 1600 cm^{-1} and another

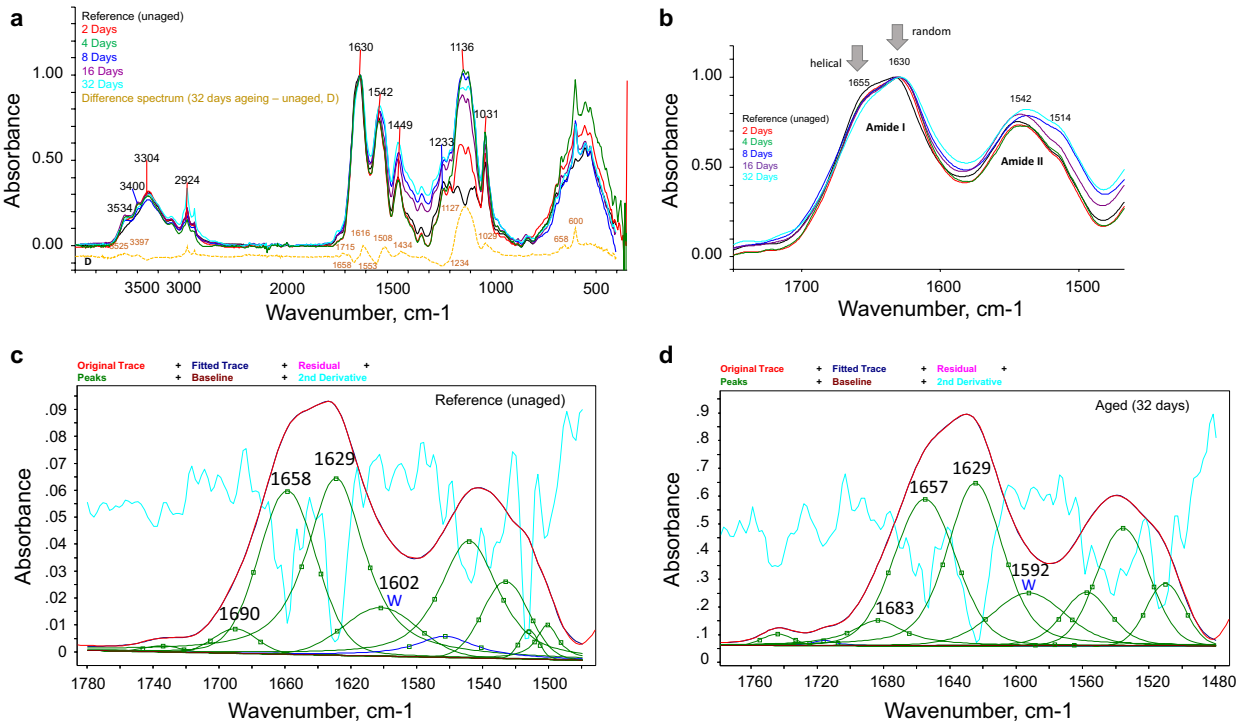

Fig. 7 ATR-FTIR spectra of ink-free parchment areas in LIG specimens at various ageing times. **a** Entire spectral region; **b** Amide I and II regions; **c** peak fitting of the amide I and II region from spectra collected from unaged specimen; **d** peak fitting of the amide I and II region in aged specimen (32 days). Spectra color in **a** and **b**: *black*: reference (unaged specimen); *red*: 2 days; *green*: 4 days; *blue*: 8 days; *purple*: 16 days; *cyan*: 32 days and *orange* (D): difference spectrum between 32 days ageing and reference. All spectra in absorbance mode; normalized to the amide I (1650–1630 cm^{-1}). Peak fitting curves in **c** and **d** marked with *w* denote the water component; *cyan* curves correspond to the second derivative

at 1581 cm^{-1} assignable to the antisymmetric Fe–O–C stretch of iron (III)—gallate complex [29] were also observed; the latter was resolved in spectra from inked areas of specimens at all ageing stages, but not from ink-free areas.

In short ageing times (4 days, Fig. 8d), Amide I is resolved in a higher number of components, with that at 1629 cm^{-1} being the strongest one, suggesting significant contribution of the unordered state. The multiple components at approximately 1690–1660 cm^{-1} possibly reflect interactions of parchment with ink components. At longer ageing times (32 days, Fig. 8e), the component at 1628 cm^{-1} is evidently the most significant, which may serve as an early indication for gelatinisation of collagen.

Specimens with LIGG formulation

Ink-free areas

The FTIR-ATR spectra from the ink-free areas (parchment areas P1 or P2 in Fig. 1) of LIGG specimens are shown in Fig. 9. A significant increase in the intensity of the sulphate band (1160–1100 cm^{-1}) due to migration from inked areas is observed, similarly to the LIG specimens. It is interesting that the higher viscosity of the ink did not prevent the effective ion migration, which, here too, is located at the surface of parchment, as spectra (not shown here) of the underlying layers (areas P3 and P5 in Fig. 1), which are exposed after scraping of the surface show no sulphate peaks.

In the difference spectrum (curve D in Fig. 9a), the calcium sulphate bands at 3516, 3398, 1124, 660 and 598 cm^{-1} are clearly evident regarding the aged specimen, together with a small increase in the intensity of the band at 1715 cm^{-1}, possibly due to liberation of carboxylic acids through hydrolysis of collagen after 32 days of ageing.

A closer look at the Amide I band shows reduced 1650 cm^{-1} helical component compared to the random coil (Fig. 9b). This is confirmed by peak fitting results (Fig. 8c, d for reference and 32 days ageing specimen, respectively) where the random coil component at 1629 cm^{-1} of Amide I is more intense in the spectra collected from samples from longer ageing times; this is also in agreement with the difference peak at 1616 cm^{-1} (curve D in Fig. 9a). A similar trend is observed in Amide II band with an increase of lower wavenumber components, again in agreement with the relatively intense difference peak at 1508 cm^{-1} (same curve in Fig. 9a). This effect is located at the surface of ink-free parchment

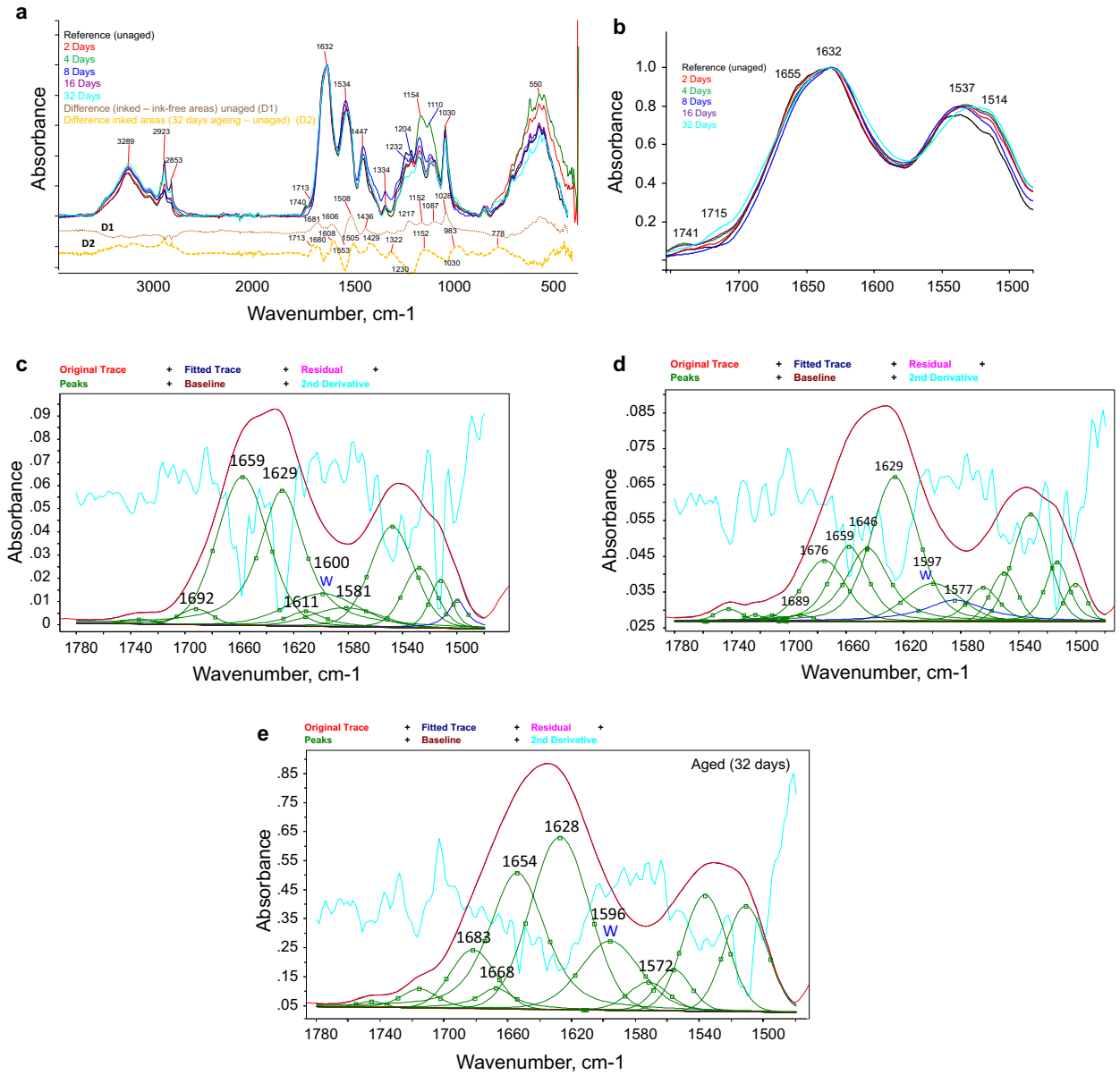

Fig. 8 ATR-FTIR spectra of inked areas in gum arabic-free LIG specimens at various ageing times. **a** Full spectra; **b** amide I and II regions; **c** peak fitting of the amide I and II region in unaged specimen; **d** peak fitting of the amide I and II region in aged specimen (4 days); **e** peak fitting of the amide I and II region in aged specimen (32 days). Spectra color in **a** and **b**: *black*: reference (unaged specimen); *red*: 2 days; *green*: 4 days; *blue*: 8 days; *purple*: 16 days; *cyan*: 32 days and *orange*: difference spectrum between 32 days ageing and reference; *brown* (D1): difference spectrum between inked and ink-free areas (both of unaged specimen) and *orange* (D2): difference spectrum between 32 days aged and reference specimens (both inked areas). All spectra in absorbance mode; normalized to the Amide I band (1650–1630 cm^{-1}). Peak fitting curves in **c**, **d** and **e** marked with *w* denote the water component; cyan curves correspond to the second derivative

areas, as spectra of the underlying layers exposed through scraping (not shown), show no such changes.

Inked areas

Spectra of inked areas (I1 in all specimens, as seen in Fig. 2) indicate ester formation with a carbonyl absorption at 1740 cm^{-1} and additional peaks due to C–O links at the 1226–1030 cm^{-1} range (Fig. 10a). The difference spectrum D1 in Fig. 10a reflects extra features in inked areas of unaged specimens (peaks at 1218, 1144, 1073 and 1030 cm^{-1}), attributed to ink and its possible interactions. These absorptions, which increase with ageing and reach their maximum intensities within the first 8 days, can be assigned to acid-catalysed formation

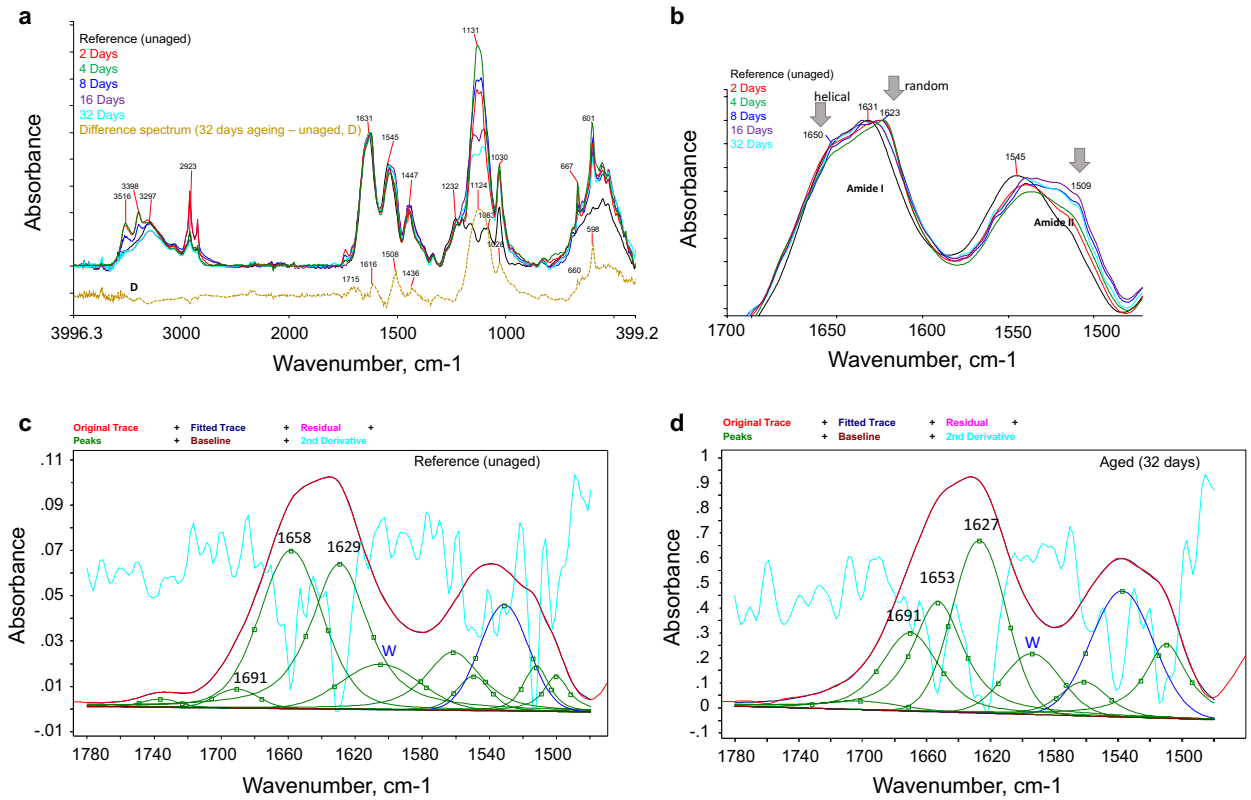

Fig. 9 ATR-FTIR spectra of ink-free parchment areas in LIGG specimens at various ageing times. **a** full spectra; **b** amide I and II regions; **c** peak fitting of the amide I and II region in unaged specimen; **d** peak fitting of the amide I and II region in aged specimen (32 days). Spectra color in **a** and **b**: *black*: reference (unaged specimen); *red*: 2 days; *green*: 4 days; *blue*: 8 days; *purple*: 16 days; *cyan*: 32 days; *orange (D)*: difference spectrum between 32 days ageing and reference. All spectra in absorbance mode; normalized to the Amide I band (1650–1630 cm^{-1}). Peak fitting curves in **c** and **d** marked with *w* denote the water component; *cyan* curves correspond to the second derivative

of esters. At longer times, a marked decrease of these bands is observed, which can be explained on the basis of subsequent ester hydrolysis under ageing conditions. Curve D2 in Fig. 10a emphasizes the formation of esters at 1742 and 1071 cm^{-1} at the second day of ageing. In addition, a broad feature at the 1200–1000 cm^{-1} range is observed, along with peaks at 660 and 600 cm^{-1} which can be assigned to calcium sulphate (cf. spectra in Figures S14, S15, Additional file 1) which is formed in this time range. The migration of sulphates is further emphasized through comparison between the inked and ink-free areas at the maximum ageing period (32 days, difference curve D3), where a large decrease at 1124, 660 and 600 cm^{-1}, assigned to calcium sulphate, is observed.

Focusing on the Amide I and II bands (Fig. 10b), a small decrease of the helical contribution at ~1650 cm^{-1} and increase of random coil at ~1630 cm^{-1} is observed upon increasing ageing time. This trend is supported through deconvolution and peak fitting. In the unaged and 2 days-aged specimens (Fig. 10c, d, respectively), two collagen chain components are resolved, similarly to other cases discussed above; of these, the helical component at ~1655 cm^{-1} is evidently stronger. This situation is reversed at longer ageing times (Fig. 10e), where the Amide I band is resolved into numerous helical components, while the random coil contribution at 1626 cm^{-1} becomes more important. This can be attributed to interactions between ink and parchment, which are more intense than those observed in inked areas of LIG formulations (see above).

In addition to the above, peak fitting of Amide II band in moderately aged specimens results in a component around 1582 cm^{-1} (similarly to corresponding spectra of LIG formulations) assignable to the antisymmetric stretch of Fe–O–C bonds in iron (III) coordination complexes [29, 67]. Prolonged ageing (32 days) caused this component to shift to lower wavenumbers (~1570 cm^{-1}), which may account for changes in the nature of its interactions [67–69] and accordingly, for the brown colour shift in all ink marks in aged parchment specimens.

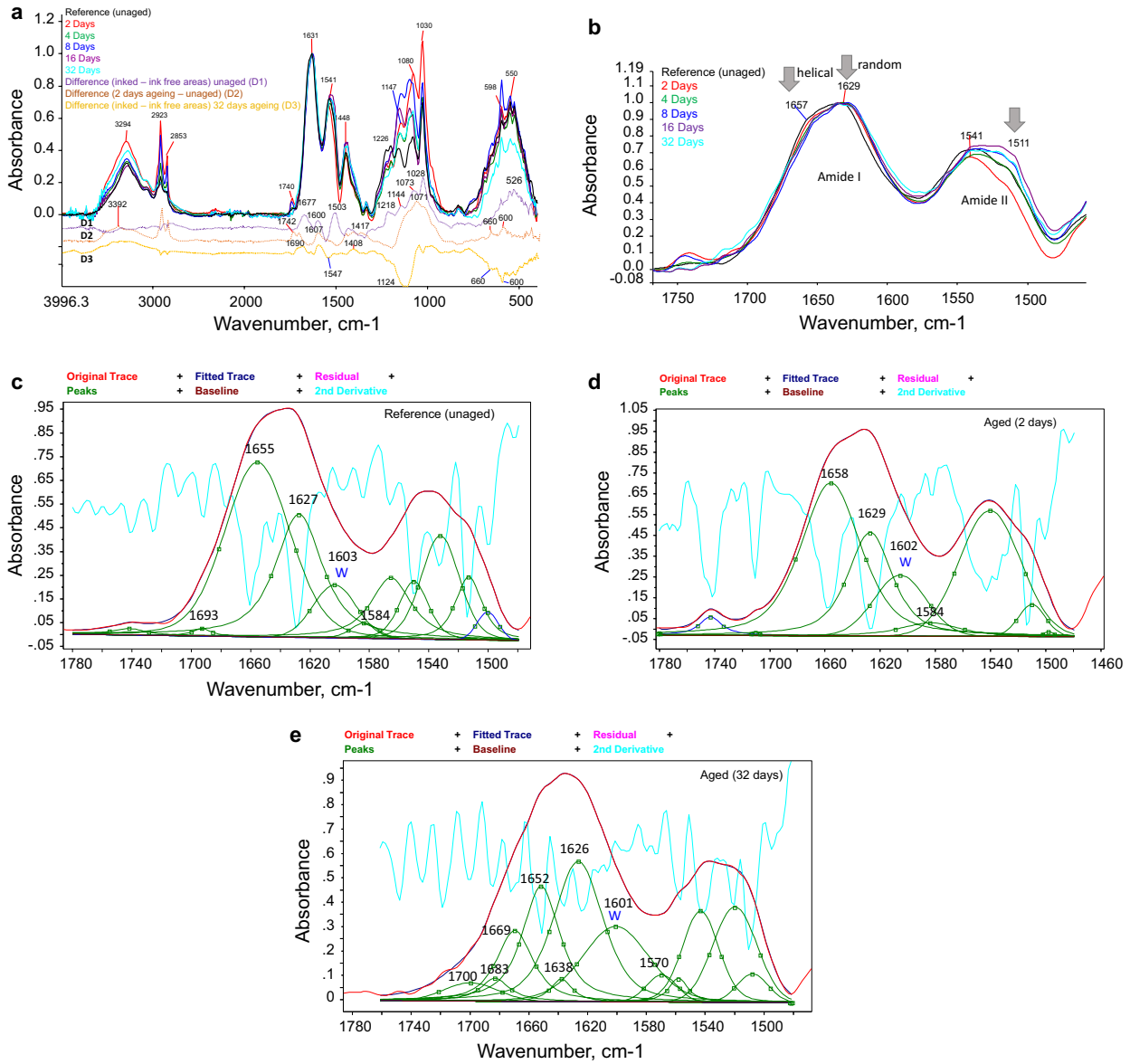

Fig. 10 ATR-FTIR spectra of inked parchment areas in LIGG specimens at various ageing times. **a** full spectra; **b** amide I and II regions; **c** peak fitting of the amide I and II region in unaged specimen; **d** peak fitting of the amide I and II region in aged specimen (2 days); **e** peak fitting of the amide I and II region in aged specimen (32 days). Spectra color in **a** and **b**: *black*: reference (unaged specimen); *red*: 2 days; *green*: 4 days; *blue*: 8 days; *purple*: 16 days; *cyan*: 32 days; *purple* (D1): difference spectrum between inked and ink-free areas, both in unaged specimens; *brown* (D2): difference spectrum between aged (2 days) and unaged specimen, both inked areas; *orange* (D3) difference spectrum between inked and ink-free areas, both in aged specimens (32 days). All spectra in absorbance mode; normalized to the Amide I band (1650–1630 cm^{-1}). Peak fitting curves in **c**, **d** and **e** marked with *w* denote the water component; *cyan* curves correspond to the second derivative

Experimental

Materials

Parchment from goat skin was acquired from Vellum-Pergamini (http://www.vellum-pergamini.com), Amfissa, Greece.

Iron (II) sulphate heptahydrate was purchased from Merck; gallic acid was purchased from Sigma; gum arabic (purchased from Exaireton, Athens).

Experimental methodology

Preparation of laboratory iron gall inks

Laboratory iron gall (LIG) inks were prepared simply by mixing iron (II) sulphate with gallic acid in deionized water. Two variations of Laboratory Iron Gall ink formulations were studied: one with only the two mentioned ingredients and no other additive, denoted as LIG ink, and another with added gum arabic, LIGG ink.

Preparation of parchment specimens

All parchment specimens (dimensions 0.6 × 1.2 cm) were selected from the backbone area, marked with the two ink formulations on the corium face of the parchment according to a scheme described below. For a reliable evaluation of results, reference samples of ink-free parchment regions in close proximity to the ink areas were analysed in parallel. Due to inhomogeneity in parchment components, the distances of sampled spots for FTIR-ATR spectroscopy between inked and ink-free areas were kept below 6 mm.

In each parchment specimen, three inked areas (I1, I2 and I3) were defined, which were separated by ink-free areas (P2, P3), (P4, P5), with areas P1 and P6 at the edges (see Fig. 2).

Two identical series of the entire parchment specimen set were prepared. Series I was analysed with SEM-EDX, with no further change. Series II was analysed with FTIR-ATR spectroscopy as follows: areas I2, I3, P3 and P5 were gently scraped with the use of a stainless steel file and were analysed with KBr-FTIR spectroscopy. Areas I1, P1, P2, P4 and P6 were analysed with ATR-FTIR spectroscopy.

Accelerated ageing

The parchment specimen series were subjected to accelerated ageing at 80 °C in the presence of humidity (RH = 80 %); ageing parameters followed the IDAP protocol [26] using climatic chamber Vötsch ATLAS-SC 340 MHG. Different parchment samples examined after 1, 2, 4, 8, 16 and 32 days of accelerated ageing.

Techniques for data analysis

Micro-hot table (MHT)

Thermal analysis—shrinkage temperature measurements were performed with a Mettler Toledo FP82HT Micro Hot Stage thermostatically controlled through a Mettler FP90 Central Processor. From each specimen area of series I, a few fibers from the corium side were isolated, imbued with deionized water and were accordingly placed on glass slides which were finally put inside the MHT sample holder.

Shrinkage activity was recorded under a microscope (Olympus C × 41 × 40 magnification). A temperature range starting from 30 °C up to 85 °C was tested with a heating rate of 2 °C/min. In all cases, five shrinkage temperature intervals were recognized, which were in accordance with previous investigations [27, 55, 65]. The onset of the third interval is termed as shrinkage temperature (T_s), or the temperature at which hydrated fibers shrink.

SEM-EDX

Samples were carbon-coated to allow for analysis with a Scanning Electron Microscope JEOL JSM-5310 with Energy Dispersive X-Ray Analyser Oxford Link Isis L310. Inked and ink-free areas in parchment samples were investigated in order to analyse the diffusion of the ink ingredients any potential in the state of degradation between these two areas. In each sample, four different spots were selected on the writing face (recto).

FTIR spectroscopy

KBr-pellets were analysed with (a): a Perkin Elmer Spectrum GX and (b) a Bruker Tensor 27 FT-IR spectrometer, both equipped with DTGS detectors. Prior to analysis, parchment material was gently scraped by means of a file and the resulting powder was mixed with KBr (at approx. 1:30 w/w ratio) and pressed to form a KBr pellet.

FTIR-ATR measurements

Fourier transform infrared spectroscopy (FT-IR) measurements were carried out using a Bruker Vertex 70v spectrometer equipped with a DTGS detector. The measurements were carried out using an A225/Q Platinum attenuated total reflection (ATR) unit with single reflection diamond crystal in the mid-IR region (350–4500 cm^{-1}) using a KBr beamsplitter.

Deconvolution and peak fitting of the Amide I and II region (1760–1484 cm^{-1}) was undertaken using the GRAMS/AI peak fitting statistics routine. In all cases, investigated region ranged at 1760–1484 cm^{-1}; baseline correction was applied in the above region; statistically converging conditions: FWHH 12 cm^{-1} with sensitivity set to medium; R^2 was 0.9993 or higher and std. error was 0.0030 or lower. In the Amide I region, two main components were resolved in most cases; one centred at 1560–1550 cm^{-1} assigned to helical components in collagen and a second one at 1632–1626 cm^{-1}, assigned to random collagen chains. In certain circumstances (see "Results and discussion" section) the helical component is was further resolved in more sub-components ranging from 1690–1650 cm^{-1}.

Conclusions

Laboratory iron gall ink-stained parchment specimens were artificially aged under moderate temperature and humidity and were studied with FTIR-ATR spectroscopy, micro-hot table thermal analysis and SEM-EDX microanalysis. After combining the analytical results, detailed information on the condition of parchment was derived based on its interactions with ink components under the ageing conditions. Thermal analysis showed no actual change in shrinkage temperatures in ink-free areas of all specimen upon ageing, until reaching 32 days, where decrease is observed. On the contrary, inked areas showed considerable decrease upon ageing, especially in formulations containing no gum arabic (LIG). In

addition, calcium sulphate crystals in both inked and ink-free parchment areas were observed through elemental micro-analysis; their presence was assigned to ion migration from inked areas to adjacent ink-free regions of the specimens.

The sulphates migration effect was confirmed and further investigated through the FTIR-ATR spectra on the inked surface of parchment specimens, which show increased presence of calcium sulphate in ink-free areas with ageing times. These eventually reach a plateau in LIG formulations. Similar phenomenon is observed in parchment specimens with gum arabic-containing ink formulations (LIGG); however in this case, the effect reaches its maximum at the first 4 days of ageing.

In all cases, close examination of Amide I band revealed reduction of the helical content (~1650 cm^{-1}) with simultaneous increase of the random coil content (~1629 cm^{-1}) further supported by deconvolution and peak fitting analysis. The Amide II band exhibited similar trend, particularly in inked areas, where one of the resolved components was assigned to iron (III)—coordinated gallate; this was shifted to lower wavenumbers upon prolonged ageing.

The combined information gained from the results of this work, offers an early sign for deterioration of the material, including gelatinisation. The results also offer a basis for further investigation on the interactions between iron gall inks with parchment. In particular, the identity of the gallate complex can be further investigated and its possible change of nature could be associated with the colour change of IGIs on parchment upon prolonged ageing. Additional techniques may also be employed, such as SDS-PAGE electrophoresis and/or chromatography to investigate possible degradation phenomena of the protein under acidic hydrolytic conditions induced by the ink environment. Finally, the results in the present work need to be compared with analogous studies of historic documents having iron gall inks on parchments.

Additional file

Additional file 1. Supplementary material containing detailed FTIR spectra from all cases of aged specimens, along with additional standard spectra.

Abbreviations

ATR: attenuated total reflection; EDX: Energy Dispersive X-ray; FTIR: Fourier transform infrared spectroscopy; IGI: iron gall ink; LIG: laboratory iron gall; LIGG: laboratory iron gall with gum arabic; MHT: micro hot table; SEM: scanning electron microscopy.

Authors' contributions

All the authors contributed in the research activities. This work was completed in two phases: phase one (experimental design, SEM, MHT and KBr-FTIR measurements as well as interpretation of data) and phase two (FTIR-ATR measurements and interpretation). EM planned the experimental design and interpreted the results of the MHT and SEM-EDX results. EM and SCB were in charge of the planning and coordination of the activities. GV prepared the formulations, and carried all measurements in stage 1. SCB carried and interpreted all measurements in stage 2 where ATR-FTIR analysis was conducted. The synthesis of the results, manuscript preparation and revision was done by SCB. All authors read and approved the final manuscript.

Acknowledgements

The authors wish to thank:
Prof. D. Anglos (university of Crete, Department of Chemistry, FORTH - IESL) for providing access and Dr. Zoi Papliaka for valuable assistance with the FTIR-ATR facility of Institute of Electronic Structure and Laser (IESL), Foundation for Research and Technology-Hellas (FORTH), P.O. Box 1385, 71110, Heraklion, Crete, Greece.

Mr. Athanasios Karabotsos (technical supervision and assistance in SEM, TEI of Athens), Dr. Alexis Stefanis, lecturer (TEI of Athens) and Dr. Agatha Kaminari adjunct lecturer (TEI of Athens), as well as Mr. Ciprian Chelaru, chemical engineer at INCDTP-ICPI (Romania), for their valuable help on experimental procedures.

The authors also wish to express their gratitude to George Kenanakis, for technical supervision, assistance and consulting in FORTH-IESL, as well as Ms Anastasia Katsidima, conservator and Antonis Douvas, researcher at NCSR-Demokritos.

Competing interests

The authors declare that they have no competing interests.

Received: 14 October 2015 Accepted: 22 April 2016
Published online: 11 May 2016

References

1. Levey M. Chemistry and chemical technology in ancient mesopotamia. Amsterdam: Elsevier; 1959.
2. Forbes RJ. Studies in ancient technology, vol V. Leiden: Brill; 1966.
3. Derrick M. Evaluation of the state of degradation of dead sea scroll samples using FT-IR spectroscopy. Book Paper Group Annual. 1991;10:1–13.
4. Olin BJ. Without comparative studies of inks, what do we know about the Vinland map? Smithsonian. 2000;2:27–36.
5. Graham R, Zubritsky E. Vinland: an inky controversy lives. Anal Chem. 2004;76:407A–12A.
6. Lee AS, Mahon PJ, Creagh DC. Raman analysis of iron gall inks on parchment. Vib Spectrosc. 2006;41:170–5.
7. Hahn O. Non-destructive investigation of the dead sea scrolls. In: 9th international conference on NDT of Art; 2008. p. 1–7. http://www.ndt.net/article/art2008/papers/243Broshi.pdf.
8. Weiner S, Kustanovich Z, Gil-Av E, Traub W. Dead Sea Scroll parchments: unfolding of the collagen molecules and racemization of aspartic acid. Nature. 1980;287:820–3.
9. Larsen R. Introduction to damage and damage assessment of parchment. In: Larsen R, editor. Improved damage assessment of parchment (IDAP): assessment, data collection and sharing of knowledge, Research Report No. 18. Copenhagen: The Royal Danish Academy of Fine Arts; 2007. p. 17–22.
10. Možir A, Gonzalez L, Kralj Cigić I, Wess TJ, Rabin I, Hahn O, Strlič M. A study of degradation of historic parchment using small-angle X-ray scattering, synchrotron-IR and multivariate data analysis. Anal Bioanal Chem. 2012;402:1559–66.
11. Haines BM. Parchment: In The physical and chemical characteristics of parchment and the materials used in its conservation, Northampton: The Leather Conservation Centre; 1999.
12. Haines BM. The manufacture of parchment. In: Kite M, Thomson R, editors. Conservation of leather and related materials. Amsterdam: Butterworth-Heinemann; 2006. p. 198–9.
13. Thomson R. Leather. In: May E, Jones M, editors. Conservation of Heritage Materials. Cambridge: RSC Publishing; 2006.

14. Susi H, Ard JS, Carroll RJ. Hydration and denaturation of collagen as observed by infrared spectroscopy. J Am Leather Chemists Assoc. 1971;66:508–19.
15. Kennedy CJ, Wess TJ. The structure of collagen within parchment—a review. Restaurator. 2003;24:61–80.
16. Bicchieri M, Monti M, Piantanida G, Sodo A, Tanasi MT. Inside the parchment. Proceedings of Art 2008, 9th International Conference. 2008. p. 25–30 http://www.ndt.net/article/art2008/papers/140Bicchieri.pdf.
17. Brodsky B, Ramshaw JAM. The collagen triple-helix structure. Matrix Biol. 1997;15:545–54.
18. Brodsky B, Werkmeister JA, Ramshaw JAM. Collagens and gelatins. Biopolymers Online. 2005. p. 119–28.
19. Gorgieva C, Kokol V. Collagen vs. gelatine-based biomaterials and their biocompatibility: review and perspectives. In: Pignatello R, editor. Biomaterials applications in nanomedicine. InTech; 2011. p. 17–52. http://www.intechopen.com/articles/show/title/collagen-vs-gelatine-based-biomaterials-and-their-biocompatibility-review-and-perspectives.
20. Engel J, Bächinger H P. Structure, stability and folding of the collagen triple helix. In: Collagen: primer in structure, processing and assembly, topics in current chemistry; 2005, 247:7–33.
21. Branden C, Tooze J. Introduction to protein structure. New York: Garland Science; 1999. p. 14.
22. Ramachandran GN, Chandrasekharan R. Interchain hydrogen bonds via bound water molecules in the collagen triple helix. Biopolymers. 1968;6:1649–58.
23. Gonzalez LG, Wess TJ. The effects of hydration on the collagen and gelatine phases within parchment artefacts. Herit Sci. 2013;1:14.
24. Mallamace F, Baglioni P, Corsaro C, Chen S-H, Mallamace D, Vasi C, Stanley H-E. The influence of water on protein properties. J Chem Phys. 2014;141:165104.
25. Patten K, Gonzalez L, Kennedy C, Mills D, Davis G, Wess T. Is there evidence for change to collagen within parchment samples after exposure to an X-ray dose during high contrast X-ray microtomography? A multi technique investigation. Herit Sci. 2013;1:22. http://www.heritagescience-journal.com/content/1/1/22.
26. Larsen R, Poulsen DV, Minddal K. Damage of parchment fibres on the microscopic level detected by the micro hot table (MHT) method. In: Larsen R, editor. Improved damage assessment of parchment (IDAP): assessment, data collection and sharing of knowledge, research report No 18. Copenhagen: The Royal Danish Academy of Fine Arts; 2007. p. 69–72.
27. Rouchon-Quillet V, Remazeilles C, Bernard J, Wattiaux A, Fournes L. The impact of gallic acid on iron gall ink corrosion. Appl Phys A Mater Sci Process. 2004;79:389–92.
28. Fazary AE, Taha M, Ju YH. Iron complexation studies of gallic acid. J Chem Eng Data. 2009;54:35–42.
29. Ponce A, Gaskell K, Brostoff L. New insights into the chemistry and structure of iron gall ink. In: New research in iron gall ink; 2012. http://www.loc.gov/preservation/outreach/symposia/igi.html.
30. Daniels V. The chemistry of iron gall ink. In The Iron Gall Ink Meeting. Newcastle-upon-Tyne: The University of Northumbria; 2000. p. 31–6.
31. Reháková M, Čeppan M, Vizárová K, Peller A, Stojkovičová D, Hricková M. Study of stability of brown-gray inks on paper support. Herit Sci. 2015;3:8. http://www.heritagesciencejournal.com/content/3/1/8.
32. Krekel C. The chemistry of historical iron gall inks. Int J Forensic Doc Exam. 1999;5:54–8.
33. Wunderlich CH. Geschichte und chemie der eisengallustinte. Restauro. 1994;100:414–21.
34. Feller R, Cheetham A. Fe(III), Mn(II), Co(II), and Ni(II) 3,4,5-trihydroxybenzoate (gallate) dihydrates; a new family of Hybrid framework materials. Solid State Sci. 2006;8:1121–5.
35. Griffiths PR, de Haseth JA. Fourier transform infrared spectrometry. Hoboken: Wiley-Interscience; 2007. p. 277–301.
36. Derrick MR, Stulik D. Infrared analysis methods. In: Infrared spectroscopy in conservation science. Chap. 4. Los Angeles: Getty Conservation Institute; 1999. p. 43–81.
37. Stuart B. Infrared spectroscopy. Fundamentals and Applications. New York: John Wiley and Sons; 2004.
38. Fringeli UP. ATR and reflectance IR spectroscopy applications. In: Tranter J, Holmes GE, Lindon J, editors. Encyclopedia of spectroscopy and spectrometry. San Diego: Academic Press; 1999. p. 58–75.
39. Glassford SE, Byrne B, Kazarian SG. Recent applications of ATR FTIR spectroscopy and imaging to proteins. Biochim Biophys Acta. 2013;1834:2849–58.
40. Kazarian SG, Chan KLA. Micro- and macro-attenuated total reflection Fourier transform infrared spectroscopic imaging. Appl Spectrosc. 2010;64:135A–52A.
41. Barth A. Infrared spectroscopy of proteins. Biochim Biophys Acta. 2007;1767:1073–101.
42. Brodsky-Doyle B, Bendit EG, Blout ER. Infrared Spectroscopy of Collagen and Collagen-Like Polypeptides. Biopolymers. 1975;14:937–57.
43. Susi H, Ard JS, Carroll RJ. Hydration and denaturation of collagen as observed by infrared spectroscopy. J Am Leather Chemists Assoc. 1971;66:508–19.
44. Barth A. The infrared absorption of amino acid side chains. Prog Biophys Mol Biol. 2000;74:141–73.
45. Payne KJ, Veis A. Fourier transform IR spectroscopy of collagen and gelatine solutions: deconvolution of the amide I band for conformational studies. Biopolymers. 1988;27:1749–60.
46. Belbachir K, Noreen R, Gouspillou G, Petibois C. Collagen types analysis and differentiation by FTIR spectroscopy. Anal Bioanal Chem. 2009;395:829–37.
47. Bandekar J. Amide modes and protein conformation. Biochim Biophys Acta. 1992;1120(2):123–43.
48. Dodd JE, de Noyer LK. Curve-fitting: modelling spectra. In: Chalmers JM, Griffiths PR, editors. Handbook of vibrational spectroscopy. Hoboken: John Wiley & Sons Ltd; 2002. p. 1033–43.
49. Jackson M, Matsch HH. The use and misuse of FTIR spectroscopy in the determination of protein structure. Crit Rev Biochem Mol Biol. 1995;30:95–120.
50. Coppola M, Djabourov M, Ferrand M. Unified phase diagram of gelatin films plasticized by hydrogen bonded liquids. Polymer. 2012;53:1483–93.
51. Odlyha M, Theodorakopoulos C, de Groot J, Bozec L, Horton M. Thermo-analytical (macro to nano-scale) techniques and non-invasive spectroscopic analysis for damage assessment of parchment. In: Larsen R, editor. Improved damage assessment of parchment (IDAP): assessment, data collection and sharing of knowledge, Research Report No. 18. Copenhagen: The Royal Danish Academy of Fine Arts; 2007. p. 73–87.
52. Odlyha M, Theodorakopoulos C, Groot JD. Fourier transform infra-red spectroscopy (ATR/FTIR) and scanning probe microscopy of parchment. e-Preserv Sci. 2009;6:138–44.
53. Vest M, Jacobsen J, Larsen R. Accelerated ageing: effect of heat and relative humidity. In: Larsen R, editor. Improved damage assessment of parchment (IDAP): assessment, data collection and sharing of knowledge, Research Report No 18. Copenhagen: The Royal Danish Academy of Fine Arts; 2007. p. 67–8.
54. Badea E, Della Gatta G, Usacheva T. Effects of temperature and relative humidity on fibrillar collagen in parchment: a micro differential scanning calorimetry (micro DSC) study. Polym Degrad Stab. 2012;97:346–53.
55. Axelsson KM, Larsen R, Sommer DVP. Dimensional studies of specific microscopic fibre structures in deteriorated parchment before and during shrinkage. J Cult Herit. 2012;13:128–36.
56. Kolar J, Štolfa A, Strlič M, Pompe M, Pihlar B, Budnar M, Simčič J, Reissland B. Historical iron gall ink containing documents—properties affecting their condition. Anal Chim Acta. 2006;555:167–74.
57. Bulska E, Wagner B. A study of ancient manuscripts exposed to iron-gall ink corrosion. Compr Anal Chem. 2004;42:755–88.
58. Oh H, Hoff J, Armstrong G, Haff L. Hydrophobic interaction in tannin-protein complexes. J Agric Food Chem. 1980;28:394–8.
59. Covington AD. The chemistry of tanning materials. In: Kite M, Thomson R, editors. Conservation of leather and related materials. Amsterdam: Butterworth-Heinemann; 2006. p. 4.
60. Madhan B, Thanikaivelan P, Subramanian V, Raghava Rao J, Nair BU, Ramasami T. Molecular mechanics and dynamics studies on the interaction of gallic acid with collagen-like peptides. Chem Phys Lett. 2001;346:334–40.
61. Axelsson KM, Larsen R, Sommer DVP, Melin R. Degradation of collagen in parchment under the influence of heat-induced oxidation: preliminary study of changes at macroscopic, microscopic, and molecular levels. Studies in conservation; 2014.

62. Dellaportas P, Papageorgiou E, Panagiaris G. Museum factors affecting the ageing process of organic materials: review on experimental designs and the INVENVORG project as a pilot study. Herit Sci. 2014;2:2. http://www.heritagesciencejournal.com/content/2/1/2.
63. Bronco S, Cappelli C, Monti S. Understanding the structural and binding properties of collagen: a theoretical perspective. J Phys Chem B. 2004;108:10101–12.
64. Yan M, Li B, Zhao X, Yi J. Physicochemical properties of gelatin gels from walleye pollock (*Theragra chalcogramma*) skin cross-linked by gallic acid and rutin. Food Hydrocoll. 2011;25:907–14.
65. Larsen R, Poulsen DV, Vest M. The hydrothermal stability (shrinkage activity) of parchment measured by the micro hot table method. In: Larsen R, editor. Microanalysis of parchment. London: Archetype Publications; 2002. p. 55–62.
66. Bicchieri M, Monti M, Piantanida G, Pinzari F, Sodo A. Non-destructive spectroscopic characterization of parchment documents. Vib Spectrosc. 2011;55:267–72.
67. Nakamoto K. Complexes of amino acids, EDTA and related compounds. Infrared and Raman spectra of inorganic and coordination compounds, Part A: theory and applications in inorganic chemistry. New York: John Wiley and Sons; 2009. p. III-7–.
68. Cirillo G, Kraemer K, Fuessel S, Puoci F, Curcio M, Spizzirri UG, Altimari I, Lemma F. Biological activity of a gallic acid-gelatin conjugate. Biomacromolecules. 2010;11:3309–15.
69. Sheena MY, Ushakumari L, Harikumar B, Varghese HT, Panicker CY. FT-IR, FT-Raman and SERS spectra of L-proline. J Iran Chem Soc. 2009;6:138–44.
70. Bi X, Li G, Doty SB, Camacho NP. A novel method for determination of collagen orientation in cartilage by Fourier transform infrared imaging spectroscopy (FT-IRIS). Osteoarthr Cartil. 2005;13:1050–8.